Bare-carbon-ion-impact electron emission from adenine molecules: Differential and total cross-section measurements

Shamik Bhattacharjee,[1] Chandan Bagdia,[1] Madhusree Roy Chowdhury,[1] Anuvab Mandal,[1] J. M. Monti,[2] Roberto D. Rivarola,[2] and Lokesh C. Tribedi[1,*]

[1]*Tata Institute of Fundamental Research, Homi Bhabha Road, Coloba, Mumbai 400005, India*

[2]*Instituto de Fisica Rosario (CONICET-UNR), Universidad Nacional de Rosario, 2000 Rosario, Argentina*

(Received 11 January 2019; revised manuscript received 23 May 2019; published 8 July 2019)

Double-differential ionization cross sections (DDCS) for bare-carbon-ion-induced ionization of vapor-phase adenine molecules ($C_5H_5N_5$) have been measured. The experiment has been performed using an electron spectroscopy technique. Electrons ejected from adenine were analyzed by a hemispherical electrostatic deflection analyzer over an energy range of 1–450 eV for emission angles from 20° to 160°. The single-differential cross section (SDCS) and total ionization cross section were also deduced. The experimental results have been compared with the continuum distorted wave-eikonal initial-state model calculation. We have observed a very good agreement between the theory and experiment. The angular distribution of the DDCS, SDCS and the asymmetry parameter for low-energy ($E_e \leqslant 0.5$ a.u.) electron display an oscillatory behavior which is in contrast to that observed in ion-atom collisions. A comparison is also made with available experimental cross-section results for uracil target colliding with the same velocity bare carbon ions and the scalability of ionization cross sections among these molecules is discussed.

DOI: 10.1103/PhysRevA.100.012703

I. INTRODUCTION

In recent times the study of ionization and fragmentation of DNA/RNA base molecules in collisions with charged projectiles have attracted increasing attention due to its growing radiobiological importance. There is a need to have a complete understanding of the series of events that take place when high-velocity radiation beams interact with the biological matter comprised of the living cells and water. Collisions of high-velocity projectiles with atoms or molecules produce a large number of secondary electrons, near the end of the projectile's trajectory, i.e., the Bragg peak (BP) region [1]. These secondary electrons can further initiate ionization events giving rise to electrons and radicals. These events triggered by the ion beam may lead to single or double strand breaks of DNA of cancer cells. The process of DNA double-strand breaks is considered to be of prime importance in producing cellular death to the cancerous cells. It is now well known that the low-energy electrons (LEE) are mainly responsible for the harmful interactions in DNA (and other biological molecules) through the process of dissociative electron attachment [2–5]. The study of energy distribution of secondary electrons emitted from biological molecules is, therefore, particularly important. Because of this reason, several investigations are taken up to study the differential and total cross sections of various breakup processes of nucleic-acid base molecules under the impact of heavy ions including protons [6–13] or water [14–19]. In general, the ejected electrons are produced from a variety of ionization processes designated as soft collisions, binary-encounter collisions, electron capture or loss to the continuum, and Auger processes [20]. The dominant ionization among these processes arises from soft (distant) collisions, which produce predominantly low-energy electrons (such as $\leqslant$50 eV—although there is no well-defined boundary).

Although the cross-section measurements for e-emission from biologically relevant molecules have gained momentum recently, the number of available results are still very scarce. Literature is especially scarce for heavy projectile ions having an energy of several MeV/u or more. The dependence of the total ionization cross section of uracil molecule on the projectile energy as well as charge state has been reported by Agnihotri *et al.*, using keV to MeV energy heavy ions [9]. For the same molecule the ionization by MeV-energy proton impact has been studied by Itoh *et al.* [12]. For adenine, differential cross-section studies were performed for 0.5, 1, and 1.5 MeV energy proton beams by Iriki *et al.* [10,11]. It may be seen that in the case of ionization of uracil by C and O ions the continuum distorted wave–eikonal initial-state (CDW-EIS) calculations show certain deviations, besides giving a qualitative agreement. To develop a comprehensive model for the trajectory calculation of such ions inside biological material one must know the degree of energy loss to estimate the radiation damage. Therefore, it is required to have an estimation of the ionization, fragmentation, or electron capture contributions towards the energy loss process in such collisons [21,22]). As, for example, no data exists for electron emission from one such nucleobase, i.e., adenine molecule, under heavy ion impact except protons. Reliable experimental data on ionization cross sections for different nucleobases under the impact of heavy ions with different incident energies are required as input to modeling the radiation damage of DNA-RNA base molecules by highly charged ion beams.

*lokesh@tifr.res.in, ltribedi@gmail.com

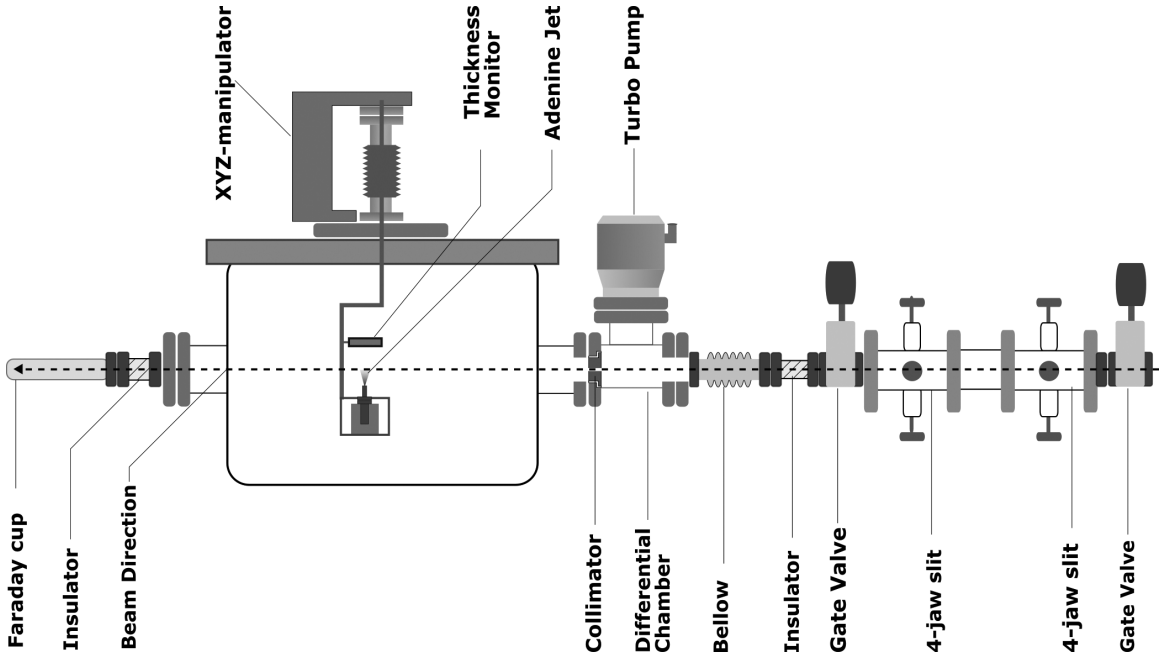

FIG. 1. Schematic drawing of the experimental setup along with part of the accelerator beamline.

In this work, we present the measurement of an absolute double-differential ionization cross section (DDCS) of vapor-phase adenine molecules ($C_5H_5N_5$) by 42 MeV C^{6+} ion impact. These results for adenine have been compared with recent theoretical values based on the CDW-EIS model. From the DDCS results, after integration, we obtained the single differential cross section (SDCS) as well as the total ionization cross-section (TCS) values. It was shown earlier that the TCS (σ) at a given proton energy is proportional to n_v for various hydrocarbon molecules up to adenine [12,23], where n_v is the number of valence electrons. So we have done a comparison of the TCS result with the earlier result on the uracil target [24] for the same projectile energy and charge state (42 MeV C^{6+}) to check the validity of such scaling.

The paper is organized as follows. In Sec. II the experimental apparatus and the techniques for deducing the DDCS results are discussed. In Sec. III we have given a brief overview of the normalization procedure used to obtain absolute DDCS. In Sec. IV, the experimental DDCS, SDCS, and TCS results are presented along with their comparisons with the CDW-EIS model. The concluding remarks are given in Sec. V.

II. MEASUREMENT TECHNIQUES

For the present work, 42 MeV C^{6+} ion beam was provided by the BARC-TIFR Pelletron accelerator facility in T.I.F.R. Mumbai. The measurements was carried out using a continuum electron spectroscopy setup. Figure 1 shows a schematic diagram of the experimental setup. The interaction chamber was kept at a base pressure of 2×10^{-7} mbar. Two μ-metal sheets having high magnetic permeability were placed inside the chamber along its perimeter to reduce Earth's magnetic field inside the chamber. This was essential for the detection of low-energy electrons which can be severely affected by Earth's magnetic field. For analyzing the ejected electron energies, a hemispherical electrostatic deflection analyzer has been used. A suitably enclosed and mounted channel electron multiplier (CEM) detected the energy analyzed electrons. This analyzer was kept on a rotatable turntable inside the chamber to detect the electrons emitted over a wide angular range. The angles of detection were chosen as 20°, 30°, 40°, 50°, 60°, 70°, 80°, 90°, 105°, 120°, 135°, 150°, and 160°. The range of electron energies has been chosen as 1–450 eV. The inner and outer electrodes of the analyzer were made of the oxygen-free high conductivity (OFHC) copper. In order to avoid the generation of the secondary electrons from the analyzer electrodes, the inner surfaces of the electrodes were coated with carbon soot. The analyzer energy resolution depends

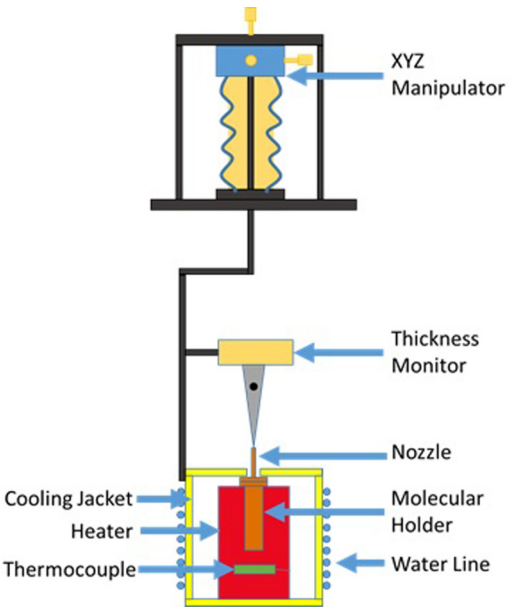

FIG. 2. Adenine jet assembly.

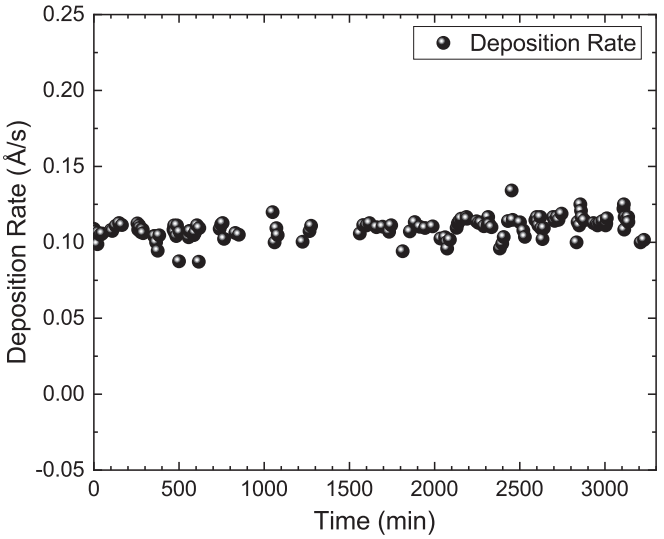

FIG. 3. Adenine vapor deposition rate throughout the experiment.

mostly on the spectrometer collimator exit slit width and the acceptance angle of the spectrometer collimator entrance slit [25] and, for the present analyzer, it is measured to be 6% of electron energy [26].

Before entering the experimental chamber, the ion beam was properly collimated by using a set of double four-jaw-slit assemblies separated one meter apart from each other. Another aperture of 4 mm radius was used just before the interaction chamber. The use of the collimator, as well as the four jaw slits, helped us in obtaining a good quality stable beam during the experiment.

The vapor target of adenine was prepared by heating the adenine powder in an oven. Figure 2 shows the schematic diagram of the jet assembly. The oven assembly consists of a cooling jacket, a quartz crystal thickness monitor, and an XYZ manipulator. The adenine was heated up to $\approx$180 °C to obtain enough vapor density in the interaction region. The molecules effuse through a nozzle of a diameter of 1 mm. Maintaining a uniform flow of vapor throughout the experiment was crucial and a challenging task. To ensure this, the oven temperature was raised very slowly and the thickness monitor was used to monitor the deposition rate in order to control the flow of molecules throughout the experiment. The thickness reading was noted at regular intervals (i.e., about every ∼5 min) throughout the experiment and the rate of deposition was monitored (Fig. 3). The variation of the deposition rate with time was smooth and it was found to vary by about 10% over about 20 h. The nitrogen-KLL-Auger emission cross section was used for absolute normalization of the adenine e-DDCS spectrum assuming the K-shell ionization cross section of N atom is the same as in the case of the N_2 target and the adenine ($C_5H_5N_5$) target. The details are given below.

III. NORMALIZATION PROCEDURE

To obtain the absolute value of the cross section, the exact determination of the number of target molecules at the interaction region is necessary. But in this kind of effusive jet experiment, it is extremely difficult to get this number reliably. To avoid this problem as well as to raise this number to the absolute scale, we used a novel method. In another experiments with the same experimental conditions and the same projectile, we obtained the absolute total $N\ KLL$ Auger cross section for the gaseous target nitrogen (N_2) by integrating the DDCS data twice in the Auger region:

$$\sigma_{\rm abs}(N-KLL,\mathrm{N_2}) = \iint_{\rm Auger}\left(\frac{d^2\sigma}{d\Omega_e d\epsilon_e}\right)d\Omega_e d\epsilon_e. \quad (1)$$

This experiment with N_2 target was performed in a flooded chamber condition for which the exact number of target molecules in the interaction region was known. The integrated DDCS term was calculated from the standard formula,

$$\frac{d^2\sigma}{d\Omega_e d\epsilon_e} = \frac{N_e/N_{pe} - N_b/N_{pb}}{n\epsilon_{el}(l\Omega)_{\rm eff}\Delta\epsilon}, \quad (2)$$

where N_e and N_b are the number of total and background counts, respectively, whereas N_{pe} and N_{pb} are the number of projectile ions in the presence and absence of target gas, respectively. The quantity $\Delta\epsilon$ is the energy resolution of the

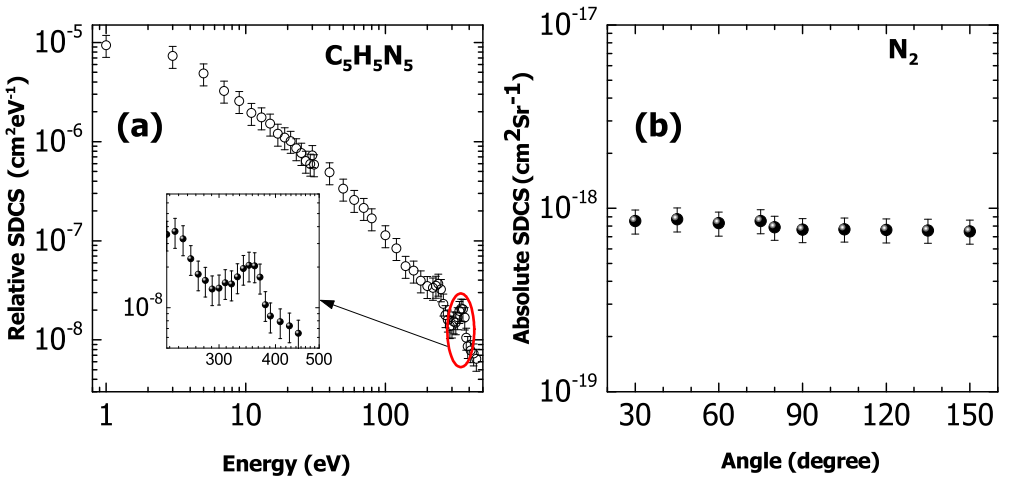

FIG. 4. Energy distribution of relative SDCS for adenine (a) and angular distribution of absolute SDCS of Auger electrons from nitrogen molecule (b). In plot (a), the inset represents the nitrogen KLL Auger electron distribution.

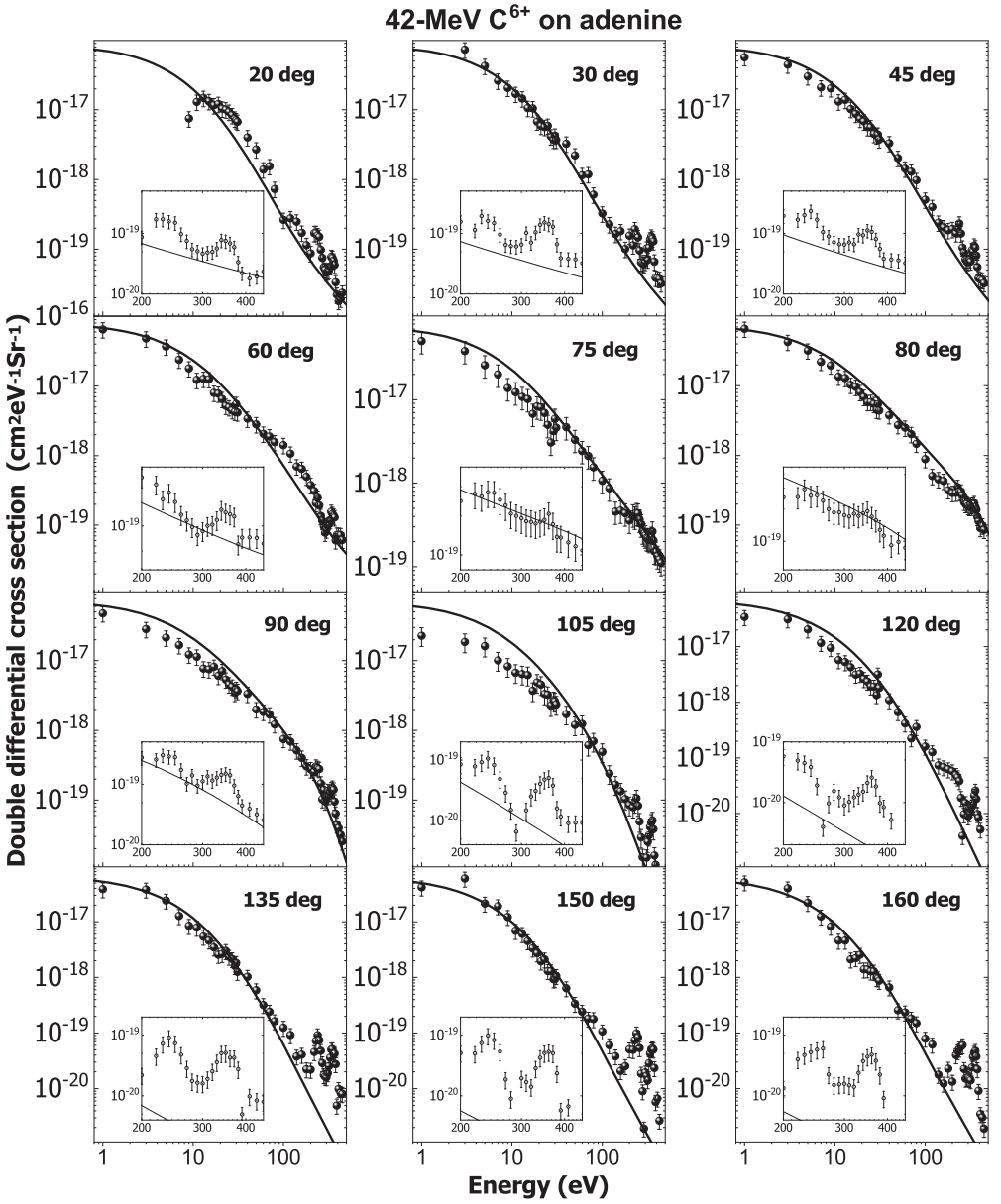

FIG. 5. Energy distributions of the e-DDCS for different emission energies for 42 MeV C^{6+} projectile. In each plot, the solid line corresponds to the CDW-EIS model calculation. The inset in each plot represents the zoomed-in plot of the Auger electron region.

spectrometer, which is 6% of the electron energy [26]. The detection efficiency of the channeltron detector (ϵ_{el}) is ≈90%. The parameter n is the target density inside the chamber and $(l\Omega)_{\text{eff}}$ is the solid angle path length integral. The SDCS angular distribution for that is displayed in Fig. 4(b).

In the second step, we determine the relative DDCS for adenine molecules from the data and the background electron counts [Fig. 4(a)]. There the solid angle path length is employed as follows:

$$\frac{d^2\sigma}{d\Omega_e d\epsilon_e} = \frac{\left(\frac{N_e(\epsilon_e\theta_e)}{N_p\Delta_\epsilon} - \frac{N_b(\epsilon_e\theta_e)}{N'_p\Delta_\epsilon}\right)}{\epsilon_{el}(l\Omega_{\text{eff}})j(\theta)}, \tag{3}$$

where the vapor density relation $j(\theta)$ is introduced because of the jet geometry [27]. From that the relative Auger cross sections for adenine were determined by

$$\sigma_{\text{rel}}(N-KLL, \text{adenine}) = \iint_{\text{Auger}} \left(\frac{d^2\sigma}{d\Omega_e d\epsilon_e}\right) d\Omega_e d\epsilon_e. \tag{4}$$

In all the cases, to get the area under the KLL line, exponential baseline subtraction was done in the single differential cross-section (SDCS) $(d\sigma/d\epsilon)$ level after performing fitting.

Now since the KLL Auger electron emission is an inner shell ionization process, we assumed that the nitrogen KLL Auger emission cross section is the same for both the N_2 and adenine after scaling by the number of N atoms. From that equality condition, we got the unknown normalization factor as given below:

$$N = \frac{\sigma_{\text{abs}}(N-KLL, N_2) \times 2.5}{\sigma_{\text{rel}}(N-KLL, \text{adenine})}. \tag{5}$$

TABLE I. DDCS ($cm^2eV^{-1}Sr^{-1}$), SDCS(θ) (cm^2Sr^{-1}), SDCS(ϵ) (cm^2eV^{-1}), and TCS (cm^2). Typical uncertainty is about 25%–30%. Numerals in square brackets indicate power of 10.

E (eV)	30°	40°	50°	60°	70°	80°	90°	105°	120°	135°	150°	$\frac{d\sigma}{d\epsilon}$
1	1.20[–16]	5.68[–17]	6.50[–17]	5.03[–17]	6.58[–17]	4.76[–17]	2.28[–17]	3.42[–17]	3.88[–17]	4.18[–17]	5.80[–16]	
5	4.26[–17]	3.01[–17]	3.68[–17]	2.58[–17]	3.20[–17]	2.14[–17]	1.62[–17]	2.05[–17]	2.43[–17]	2.14[–17]	3.00[–16]	
9	2.06[–17]	2.03[–17]	1.79[–17]	1.38[–17]	1.95[–17]	1.22[–17]	8.26[–18]	9.49[–18]	8.47[–18]	1.23[–17]	1.58[–16]	
13	1.45[–17]	1.38[–17]	1.27[–17]	1.08[–17]	1.29[–17]	7.71[–18]	6.40[–18]	5.28[–18]	5.42[–18]	6.06[–18]	1.08[–16]	
17	1.05[–17]	8.76[–18]	7.99[–18]	6.77[–18]	9.62[–18]	8.17[–18]	3.70[–18]	3.14[–18]	3.47[–18]	3.32[–18]	7.41[–17]	
21	5.89[–18]	6.81[–18]	6.50[–18]	8.08[–18]	6.90[–18]	7.08[–18]	4.53[–18]	2.62[–18]	2.64[–18]	1.94[–18]	6.26[–17]	
30	4.26[–18]	4.41[–18]	5.54[–18]	5.90[–18]	5.44[–18]	3.92[–18]	2.62[–18]	3.17[–18]	1.82[–18]	9.35[–19]	4.49[–17]	
40	3.26[–18]	3.31[–18]	3.39[–18]	4.69[–18]	3.77[–18]	3.33[–18]	1.71[–18]	1.09[–18]	1.03[–18]	6.42[–19]	3.03[–17]	
60	1.15[–18]	1.43[–18]	2.06[–18]	2.43[–18]	2.50[–18]	1.84[–18]	1.24[–18]	4.17[–19]	3.19[–19]	2.42[–19]	1.59[–17]	
80	6.07[–19]	9.78[–19]	1.56[–18]	1.55[–18]	1.47[–18]	1.22[–18]	6.97[–19]	3.61[–19]	1.64[–19]	1.78[–19]	1.04[–17]	
100	3.24[–19]	5.12[–19]	1.41[–18]	1.07[–18]	8.86[–19]	7.50[–19]	4.90[–19]	1.59[–19]	1.24[–19]	1.07[–19]	6.99[–18]	
120	2.28[–19]	4.02[–19]	1.06[–18]	8.68[–19]	5.06[–19]	6.92[–19]	2.39[–19]	1.27[–19]	9.21[–20]	6.05[–20]	5.19[–18]	
140	1.65[–19]	2.40[–19]	6.98[–19]	4.57[–19]	4.55[–19]	5.15[–19]	1.67[–19]	7.33[–20]	3.80[–20]	3.82[–20]	3.43[–18]	
160	1.81[–19]	2.06[–19]	6.46[–19]	4.70[–19]	4.31[–19]	4.03[–19]	1.34[–19]	6.81[–20]	4.07[–20]	2.08[–20]	3.09[–18]	
180	1.01[–19]	1.87[–19]	4.95[–19]	4.36[–19]	3.16[–19]	3.04[–19]	1.03[–19]	6.26[–20]	2.22[–20]	2.55[–20]	2.45[–18]	
200	1.56[–19]	1.94[–19]	3.77[–19]	3.57[–19]	2.89[–19]	2.76[–19]	8.49[–20]	5.76[–20]	2.19[–20]	5.09[–20]	2.15[–18]	
220	1.13[–19]	1.69[–19]	3.10[–19]	4.24[–19]	2.91[–19]	2.55[–19]	7.89[–20]	4.93[–20]	4.55[–20]	4.99[–20]	2.07[–18]	
250	1.48[–19]	1.68[–19]	1.93[–19]	4.34[–19]	3.03[–19]	2.79[–19]	8.31[–20]	1.92[–20]	7.42[–20]	8.35[–20]	2.00[–18]	
270	6.48[–20]	8.91[–20]	1.16[–19]	3.22[–19]	2.17[–19]	1.03[–19]	2.91[–20]	9.70[–21]	2.86[–20]	1.86[–20]	1.09[–18]	
290	6.11[–20]	6.63[–20]	7.80[–20]	2.51[–19]	2.01[–19]	9.55[–20]	6.58[–21]	1.22[–20]	1.64[–20]	1.93[–21]	8.49[–19]	
310	1.02[–19]	7.11[–20]	1.00[–19]	2.21[–19]	1.82[–19]	1.35[–19]	1.49[–20]	1.02[–20]	1.90[–20]	1.68[–20]	9.45[–19]	
330	1.05[–19]	9.66[–20]	1.18[–19]	2.10[–19]	1.84[–19]	1.29[–19]	3.12[–20]	1.35[–20]	3.60[–20]	2.84[–20]	1.04[–18]	
350	1.52[–19]	1.12[–19]	1.44[–19]	2.28[–19]	2.06[–19]	1.50[–19]	4.78[–20]	2.11[–20]	5.12[–20]	5.10[–20]	1.28[–18]	
370	1.29[–19]	8.09[–20]	1.29[–19]	2.06[–19]	1.66[–19]	9.53[–20]	3.82[–20]	1.84[–20]	4.27[–20]	5.06[–20]	1.04[–18]	
390	3.89[–20]	3.83[–20]	7.26[–20]	1.50[–19]	1.14[–19]	4.45[–20]	1.17[–20]	8.40[–21]	4.97[–21]	5.76[–21]	5.33[–19]	
410	3.81[–20]	3.70[–20]	7.27[–20]	1.34[–19]	9.06[–20]	3.96[–20]	9.12[–21]	5.16[–21]	9.86[–21]	6.68[–21]	4.84[–19]	
430	3.72[–20]	3.59[–20]	7.19[–20]	1.23[–19]	9.84[–20]	3.19[–20]	9.26[–21]	–1.84[–21]	8.36[–21]	2.67[–21]	4.50[–19]	
450	3.22[–20]	3.24[–20]	6.15[–20]	1.11[–19]	8.52[–20]	2.55[–20]	9.20[–21]	–5.53[–22]	8.00[–21]	5.01[–22]	3.97[–19]	
$\frac{d\sigma}{d\Omega}$	7.66[–16]	6.20[–16]	7.47[–16]	7.02[–16]	7.23[–16]	5.51[–16]	3.20[–16]	2.99[–16]	3.23[–16]	3.66[–16]	6.08[–15] (TCS)	

The factor 2.5 in the numerator accounts for the fact that the adenine molecule ($C_5H_5N_5$) has five nitrogen atoms, while the nitrogen molecule has only two. As the continuum part of the DDCS spectra as well as the Auger peak were produced from the same target density, jet profile, bean overlap, and other unknown experimental parameters, we could use the same absolute normalization factor as well to raise the continuum part to an absolute scale, i.e.,

$$\mathrm{DDCS_{abs}} = N \times \mathrm{DDCS_{rel}}. \quad (6)$$

Further details of the normalization procedure are available in [28]. The overall uncertainty in these absolute cross-section measurements was estimated to be about 25% –30%, which mainly arises from the adenine vapor density fluctuation (10%–15%), normalization procedure (15%–18%), the statistical uncertainty (about 5%), solid-angle path length (8%–10%), etc. It may be mentioned here that possible influence of the inter-Coulombic decay (ICD) or the ICD-like processes involving core- holes on *KLL* Auger electron emission has not been considered here. For more details one may refer to the review by Jahnke [29] and also the work by Harbach *et al.* [30] for a possible role of the ICD in radiobiology.

IV. EXPERIMENTAL RESULTS

A. Double differential cross sections

1. Energy distribution

Figure 5 shows the obtained DDCS energy distribution results at twelve different electron emission angles between 20° and 160°, while Table I displays the experimentally obtained DDCS values. All of the spectra indicate a monotonic decrease with the increasing electron energy, except for the two peaks in the higher-energy region. Two peaks located at about 250 and 400 eV are *KLL* Auger electrons ejected from carbon and nitrogen, respectively. The cross section reaches a large value in the low (<15 eV) energy region due to the dominance of the soft collision process involving a large impact parameter. The cross section then decreases over several orders of magnitude with the increase in the emission energy.

The experimental data have been compared with the CDW-EIS model calculations. The molecular structure of the adenine target was determined with the Gaussian 09 software at the restricted Hartree-Fock (RHF)/3-21G level of theory with geometrical optimization. Then, the complete neglect of differential overlap (CNDO) approximation was employed to determine the effective occupation analysis of the different atomic compounds of the molecular orbitals. Thus differential cross sections for each molecular orbital were obtained as

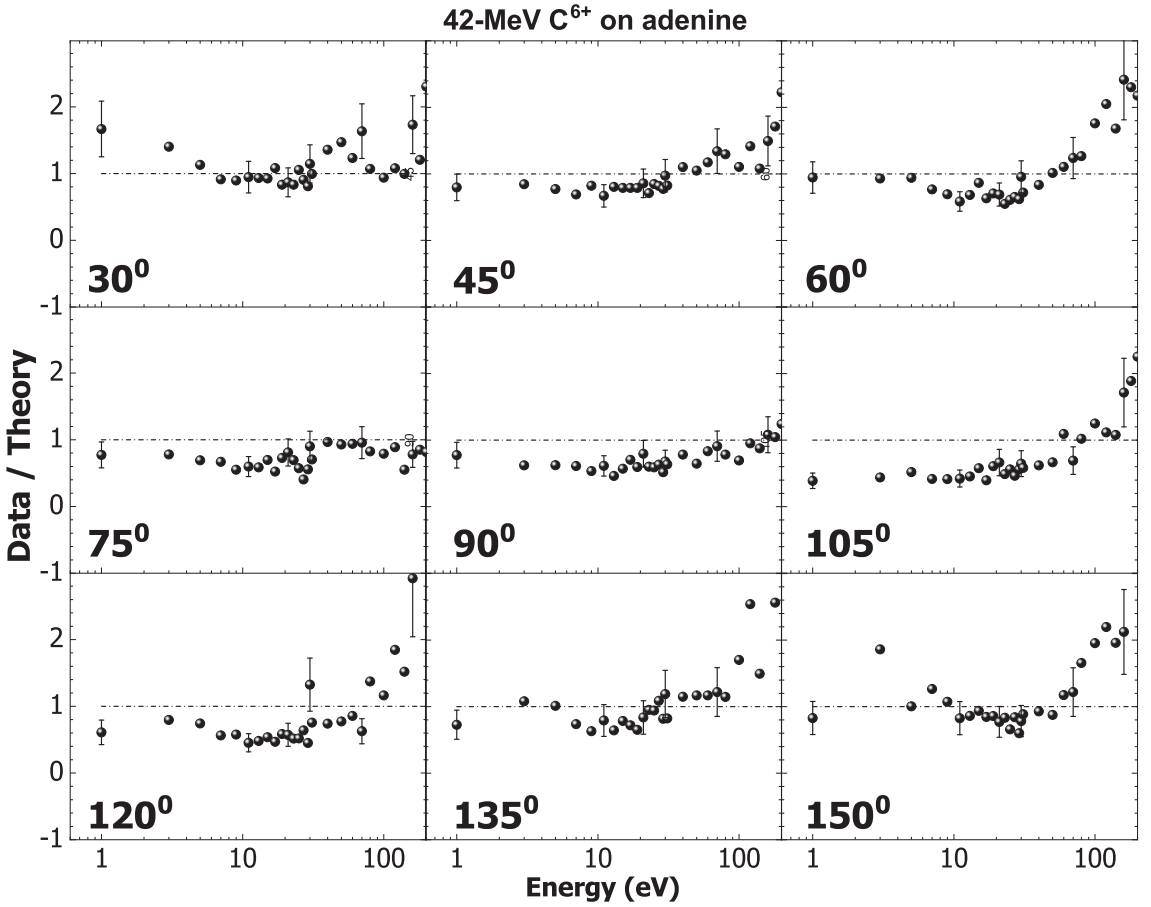

FIG. 6. Ratio of experimental-to-theoretical DDCS. A dash-dotted line represents the expected ratio, i.e., unity.

a sum of the corresponding atomic compounds (see [31] for a detailed description of the model here used). In the present work the prior version of the CDW-EIS model has been employed [17]. This prior version of CDW-EIS improves the post one, which has been largely employed to calculate electron ionization cross sections of water and nucleobases by ion impact. It was shown that the CDW-EIS post version does not include the influence of the dynamic evolution of the nonionized target electrons on the ejected one, which on the contrary is taken into account in the prior version. The important role played by this interaction between the passive electrons and the active one on DDCS calculations was demonstrated for atomic [32–34] and for water targets [17,35]. Thus, as the prior version of CDW-EIS contains more complete physical information than the corresponding post version, the prior one was adopted in the present work to study ionization of the here considered nucleobases. A very good quantitative agreement between the theory and experiment could be seen for almost all the emission angles. In particular, near perfect agreement is visible for the data obtained at 20°, 30°, 45°, 80°, 135°, 150°, and 160° throughout the entire e-energy range. In case of 60°, although the model goes through the data points, a slight periodic deviation may be noted. Similarly, in the angular range of 90° to 120°, one finds small deviations in the low-energy part of the spectrum. In general, an excellent agreement observed over almost all angular and energy ranges is remarkable, which has not been observed for earlier DDCS studies of uracil or adenine, particularly by such heavy ions. In that sense this better agreement between the theoretical and experimental investigations of ion-induced ionization can be encouraging to provide reliable input to the simulations (e.g., Refs. [21,22]) of the charged particle trajectory inside biological matter including water. To better visualize the difference between experimental data and the theoretical model, the obtained data have been divided by the corresponding theoretical values at each emission energy (see Fig. 6). From the figure, it is clear that for the forward angles the ratio is close to unity (within a maximum of about 40%) for most of the energies in the intermediate energy region (i.e., up to about 100 eV). At highest energy, i.e., around 200 eV the deviation increases to a factor of 2 to 3. These are more evident for all backward angles. Therefore, although there is overall good qualitative agreement with the model some limitations are also displayed in these plots.

2. Angular distribution

Figure 7 shows the angular distributions of the e-DDCS for several electron energies. Very low-energy electrons (<20 eV) display a decreasing trend with angle which is well reproduced by the calculation. However, a closer inspection reveals an oscillatory behavior for lower-energy electrons, i.e., below about 15 eV or 0.5 a.u. (i.e., electron velocity of 1 a.u.), which gradually vanishes at higher energies. For electrons

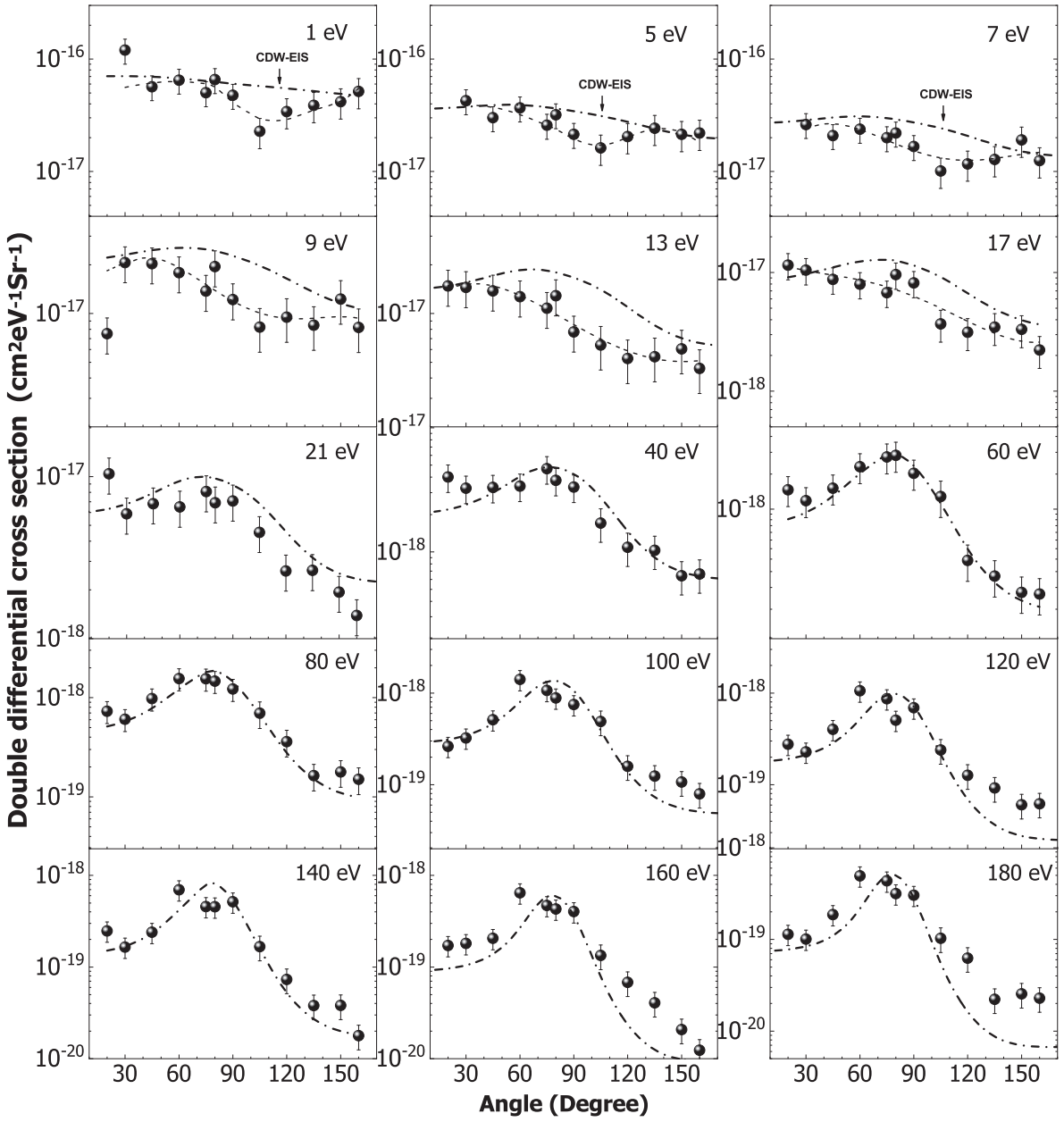

FIG. 7. Angular distributions of the e-DDCS for different emission energies. The dash-dotted line corresponds to the CDW-EIS model calculation. In the case of the top six panels, i.e., 1 to 17 eV, the dashed lines are a guide to the eyes to denote oscillatory behavior for the data up to 13 eV.

above 20 eV, a peak starts to appear for angles close to 80°. This nature becomes more prominent as the electron energy increases. The peak appears to become sharper for higher energies. This behavior is of course well known in ion-atom collisions and is a signature of the binary nature of the collision. Comparison with the CDW-EIS model shows a very good agreement with the data, especially in the higher-energy region. In Fig. 7 it can be seen that we have noticed that, for higher-energy secondary electrons, there is a substantial difference between the DDCS values for extreme forward and backward angles. This forward-backward asymmetry, in the case of ion-atom collisions, arises because of the well-known two-center electron emission process (TCEE) and the postcollision interaction (PCI) apart from the non-Coloumb target potential. In order to quantify this angular asymmetry, we have calculated and plotted a single parameter, i.e., the forward-backward asymmetry parameter $\alpha(v_e, \theta)$, defined as

$$\alpha(v_e\theta) = \frac{\sigma(v_e, \theta) - \sigma(v_e, \pi - \theta)}{\sigma(v_e, \theta) + \sigma(v_e, \pi - \theta)}. \tag{7}$$

Here $\sigma(v_e, \theta)$ and $\sigma(v_e, \pi - \theta)$ represent the e-DDCS values for a forward angle θ and the corresponding complementary (backward) angle $(\pi - \theta)$, respectively. Figure 8 shows the asymmetry parameter $[\alpha(v_e, \theta)]$ as a function of ejected electron velocity (v_e, in a.u.) deduced from the e-DDCS measured at angles 30° and 150°. The plot shows a rise in the asymmetry parameter as the electron velocity increases. For very

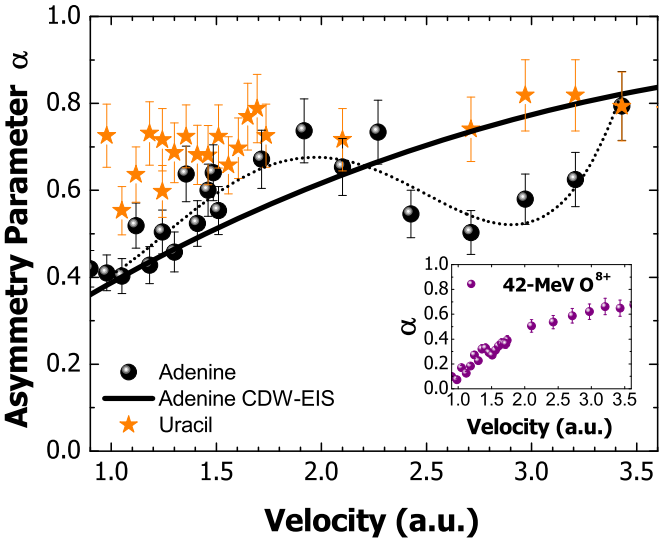

FIG. 8. Forward-backward asymmetry parameter for e-emission from adenine (solid circles) as a function of v_e along the CDW-EIS model prediction (solid line). The similar data for uracil ("star") and oxygen targets (inset) colliding with the same projectile at the same energy are also shown. The dotted line in the figure represents a guide to the eye for the adenine data which reveals an oscillatory behavior.

low-energy electrons, e.g., for $v_e = 1$ a.u., the value is around 0.4 (in Fig. 8). This asymmetry parameter is sensitive to the beam energy, charge state as well as non-Coulomb potential, and the target (molecular) wave function. This parameter, however, begins to saturate at a value of ≈0.9 for electron energy >100 eV. The asymmetry plots for uracil show slightly different behavior as the asymmetry parameter is nearly flat. It should be noticed that, in the case of the adenine, there is an oscillatory behavior in the asymmetry parameter values. The dotted line in Fig. 8 represents a guide to the eye for this oscillation behavior. This behavior is generally not observed for ion-atom collisions. Even for the uracil target which has only one benzene ring such oscillation does not arise. It is to be investigated whether this oscillation arises due to the structure of adenine molecule, which involves another second ring fused with the benzene ring. It may be noted that, due to Young-type electron interference at a molecular double slit, such as H_2 [36] or N_2 [37], one observed oscillation in the asymmetry parameter. The interference oscillation has also been observed in relatively bigger molecules, such as hydrocarbon molecules, and has been applied towards the precise estimation of the bond length [38]. In the present case, however, the explanation of the observed asymmetry may involve a more complicated mechanism which cannot be exactly identified at this stage. The inset in Fig. 8 represents the asymmetry parameter plot for the O_2 target colliding with same velocity bare carbon ions. From the inset, it can be observed that the asymmetry distribution is of a different shape when compared with heavier targets like uracil or adenine. The data for the O_2 molecule show a very steep rise in asymmetry with respect to secondary electron energy. This behavior is expected based on the two center effect in ion-atom or ion-simple molecule collisions. This nature is different than those observed for heavy target molecules, such as adenine or uracil, for which

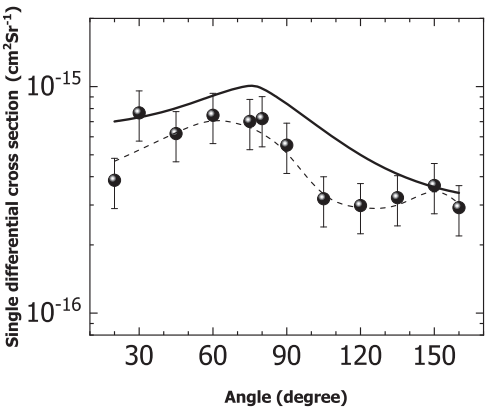

FIG. 9. Angular distribution of e-SDCS and the corresponding CDW-EIS calculation. Dashed line is a guide to the eyes.

the asymmetry is even larger in the low electron velocity region.

B. Single differential cross section

Figures 9 and 10, respectively, display the energy and angular distributions of the SDCS in the case of the adenine target. The angular distribution of the SDCS ($d\sigma/d\Omega$) has been obtained after numerically integrating the DDCS values over the emitted electron energy. The energy distribution of the SDCS ($d\sigma/d\epsilon$) has been obtained after integrating DDCS values over the electron emission angle. Both the energy and angular distribution of the SDCS have been compared with the CDW-EIS model calculation. The CDW-EIS model agrees reasonably well with the experimental results for $d\sigma/d\Omega$, although, in general, a slight overestimation of experimental results by the theoretical model can be observed. The shape of the calculated distribution also slightly differs from the experimental data. The oscillatory structure observed in the distribution is obvious (see the dashed line as a guide to the eyes). The exact mechanism for this cannot be identified. This

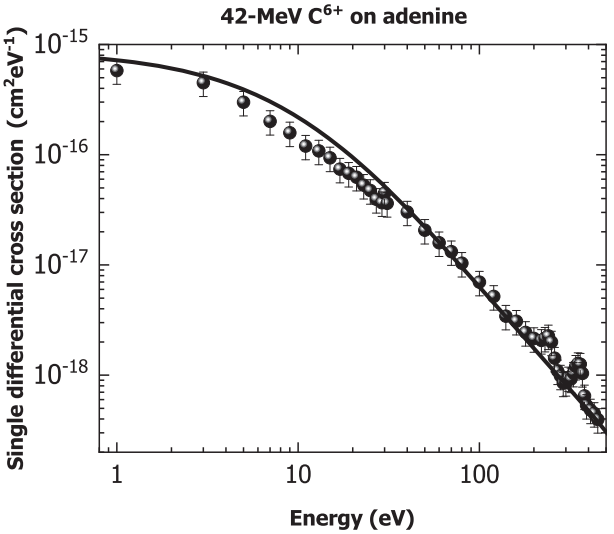

FIG. 10. Energy distribution of the e-SDCS along with the CDW-EIS calculations for adenine.

TABLE II. Total ionization cross section in units of 10^3 Mb. The uncertainty in the TCS values are about 25%.

Projectile	Expt. (>1 eV)	Expt. (>20 eV)	CDW-EIS (>20 eV)	CDW-EIS (>1 eV)
42 MeV C^{6+}	6.07	2.29	2.54	8.25

needs to be investigated in the future. As far as the $(d\sigma/d\epsilon)$ is concerned, the CDW-EIS model very well reproduces the sharp fall but slightly overestimates the experimental results till 30 eV. Above 30 eV, a very good agreement can be seen. The two Auger peaks (for C and N) are also visible in the SDCS energy distribution spectrum.

C. Total ionization cross sections

Total cross sections were obtained by integrating the SDCS values over the electron emission angle or the emitted electron energies. The integration is done for the entire angular range, from 0° to 180°. As the data is not available below 20° and above 160°, those values have been obtained by extrapolating the data for extreme forward and extreme backward. For this purpose we used the CDW-EIS as a guideline to give the slope of the experimental distribution near 0° and 180°. Observing a nearly flat distribution in the theory we assumed the SDCS value at 0° to be the same as at 20° and similarly those at 160° and 180° were assumed to be the same. Under this assumption the contributions of these "missing" angles to the TCS were found to be about 5(±0.5)%. Since this contribution is much less than the TCS, this error will have negligible contribution to the total uncertainty in the TCS. Table II shows the obtained TCS values and their comparison with the CDW-EIS model calculations. As was mentioned earlier it is the low-energy electrons (LEE) that contribute mainly towards the cellular damage to cancer cells [2–5]. The table shows that the secondary electrons having energies <20 eV constitute the maximum, i.e., as large as 70% of the total emitted electrons, which is close to what the theory also suggests.

The scaling property for proton impact ionization cross sections of various hydrocarbons were investigated by Toburen *et al.* [23]. It was found that the ionization cross sections can be scaled according to their valence electron numbers. Later Itoh *et al.* showed that their cross-section results for adenine and uracil can also be scaled reasonably well according to this scaling law [10,12]. This happens because, during ionization, it is the loosely bound outer electrons that contribute the most. This valence electron scaling can also be checked by comparing our present adenine results with the existing result for uracil target [28]. Adenine has a total of 50 valence electrons, while uracil has 42 valence electrons. So according to valence electron scaling the $\sigma_{\text{adenine}}/\sigma_{\text{uracil}}$ should be 1.2. The experimentally obtained ratio of 1.5 ± 0.4 thus agrees with this number, considering the experimental uncertainty.

V. CONCLUSIONS

We have measured energy and angular distribution of the electron DDCS in ionization of adenine molecule in collisions with 3.5 MeV/u bare C ions. The single differential cross sections ($d\sigma/d\Omega$ and $d\sigma/d\epsilon_e$) and total ionization cross section have also been deduced. The lowest-energy electrons (<40 eV) which are mainly responsible for radiation damage are found to constitute almost 70% of the total electron emission cross section. The experimental results have been compared with the CDW-EIS model. The overall energy and angular distributions of the measured DDCS reveal an excellent qualitative agreement with the theoretical model. However, certain deviations of the model prediction from the experimental data are also observed from the DDCS ratios. The energy distribution of the SDCS shows a very good agreement with the theoretical model although the SDCS angular distribution shows some deviations from theory. The angular distributions of the electron DDCS, measured at lower energies, showed oscillatory structure which is in contrast to the smooth behavior observed in collisions with small molecules. The observed large forward enhancement and backward depletion of electrons emitted with low energy was quite different than that observed for lighter targets, such as O_2. In addition the asymmetry parameter reveals an oscillatory structure which was absent in the case of RNA-based molecule uracil, which has a single-benzene ring. Finally, by comparing the TCS result for adenine and uracil, we find that these can be approximately scaled according to their valence electron numbers, as predicted earlier.

[1] L. Sanche, Mass Spectrom. Rev. **21**, 349 (2002).
[2] B. Boudaïffa, P. Cloutier, D. Hunting, M. A. Huels, and L. Sanche, Science **287**, 1658 (2000).
[3] S. Gohlke, A. Rosa, E. Illenberger, F. Bruning, M. A. Huels *et al.*, J. Chem. Phys. **116**, 10164 (2002).
[4] H. Abdoul-Carime, S. Gohlke, and E. Illenberger, Phys. Rev. Lett. **92**, 168103 (2004).
[5] C. König, J. Kopyra, I. Bald, and E. Illenberger, Phys. Rev. Lett. **97**, 018105 (2006).
[6] P. Moretto-Capelle and A. Le Padellec, Phys. Rev. A **74**, 062705 (2006).
[7] J. Tabet, S. Eden, S. Feil, H. Abdoul-Carime, B. Farizon, M. Farizon, S. Ouaskit, and T. D. Märk, Phys. Rev. A **81**, 012711 (2010).
[8] J. Tabet, S. Eden, S. Feil, H. Abdoul-Carime, B. Farizon, M. Farizon, S. Ouaskit, and T. D. Märk, Phys. Rev. A **82**, 022703 (2010).
[9] A. N. Agnihotri, S. Kasthurirangan, S. Nandi, A. Kumar, M. E. Galassi, R. D. Rivarola, O. Fojón, C. Champion,

J. Hanssen, H. Lekadir *et al.*, Phys. Rev. A **85**, 032711 (2012).
[10] Y. Iriki, Y. Kikuchi, M. Imai, and A. Itoh, Phys. Rev. A **84**, 032704 (2011).
[11] Y. Iriki, Y. Kikuchi, M. Imai, and A. Itoh, Phys. Rev. A **84**, 052719 (2011).
[12] A. Itoh, Y. Iriki, M. Imai, C. Champion, and R. D. Rivarola, Phys. Rev. A **88**, 052711 (2013).
[13] B. Rudek, D. Bennett, M. U. Bug, M. Wang, W. Y. Baek, T. Buhr, G. Hilgers, C. Champion, and H. Rabus, J. Chem. Phys. **145**, 104301 (2016).
[14] D. Ohsawa, Y. Sato, Y. Okada, V. P. Shevelko, and F. Soga, Phys. Rev. A **72**, 062710 (2005).
[15] F. Gobet, S. Eden, B. Coupier, J. Tabet, B. Farizon, M. Farizon, M. J. Gaillard, M. Carré, S. Ouaskit, T. D. Märk, and P. Scheier, Phys. Rev. A **70**, 062716 (2004).
[16] C. Dal Cappello, C. Champion, O. Boudrioua, H. Lekadir, Y. Sato, and D. Ohsawa, Nucl. Instrum. Methods Phys. Res., B **267**, 781 (2009).
[17] S. Nandi, S. Biswas, A. Khan, J. M. Monti, C. A. Tachino, R. D. Rivarola, D. Misra, and L. C. Tribedi, Phys. Rev. A **87**, 052710 (2013).
[18] S. Bhattacharjee, S. Biswas, C. Bagdia, M. Roychowdhury, S. Nandi, D. Misra, J. M. Monti, C. A. Tachino, R. D. Rivarola, C. Champion *et al.*, J. Phys. B **49**, 065202 (2016).
[19] S. Bhattacharjee, C. Bagdia, M. R. Chowdhury, J. M. Monti, R. D. Rivarola, and L. C. Tribedi, Eur. Phys. J. D **72**, 15 (2018).
[20] N. Stolterfoht, R. D. DuBois, and R. D. Rivarola, *Electron Emission in Heavy Ion-atom Collisions* (Springer Science and Business Media, New York, 2013), Vol. 20 .
[21] M. A. Quinto, J. M. Monti, P. F. Weck, O. A. Fojón, J. Hanssen, R. D. Rivarola, P. Senot, and C. Champion, Eur. Phys. J. D **71**, 130 (2017).
[22] A. Verkhovtsev, A. Traore, A. Muñoz, F. Blanco, and G. Garcia, Radiat. Phys. Chem. **130**, 371 (2017).
[23] D. Lynch, L. Toburen, and W. Wilson, J. Chem. Phys. **64**, 2616 (1976).
[24] A. N. Agnihotri, S. Kasthurirangan, S. Nandi, A. Kumar, C. Champion, H. Lekadir, J. Hanssen, P. F. Weck, M. E. Galassi, R. D. Rivarola *et al.*, J. Phys. B **46**, 185201 (2013).
[25] K. Sevier, *Low Energy Electron Spectrometry* (Wiley, New York, 1972).
[26] D. Misra, K. V. Thulasiram, W. Fernandes, A. H. Kelkar, U. Kadhane, A. Kumar, Y. Singh, L. Gulyas, and L. C. Tribedi, Nucl. Instrum. Methods Phys. Res., B **267**, 157 (2009).
[27] G. Scoles, *Atomic and Molecular Beam Methods* (Oxford University Press, New York, 1988), Chap. 4, pp. 83–90.
[28] A. N. Agnihotri, S. Nandi, S. Kasthurirangan, A. Kumar, M. E. Galassi, R. D. Rivarola, C. Champion, and L. C. Tribedi, Phys. Rev. A **87**, 032716 (2013).
[29] T. Jahnke, J. Phys. B **48**, 082001 (2015).
[30] P. H. P. Harbach, M. Schneider, S. Faraji, and A. Dreuw, J. Phys. Chem. Lett. **4**, 943 (2013).
[31] M. E. Galassi, C. Champion, P. F. Weck, R. D. Rivarola, O. Fojón, and J. Hanssen, Phys. Med. Biol. **57**, 2081 (2012).
[32] J. M. Monti, O. A. Fojón, J. Hanssen, and R. D. Rivarola, J. Phys. B **43**, 205203 (2010).
[33] J. M. Monti, O. A. Fojón, J. Hanssen, and R. D. Rivarola, J. Phys. B **46**, 145201 (2013).
[34] S. Biswas, D. Misra, J. M. Monti, C. A. Tachino, R. D. Rivarola, and L. C. Tribedi, Phys. Rev. A **90**, 052714 (2014).
[35] C. A. Tachino, J. M. Monti, O. A. Fojón, C. Champion, and R. D. Rivarola, J. Phys. B **47**, 035203 (2014).
[36] D. Misra, A. Kelkar, U. Kadhane, A. Kumar, L. C. Tribedi, and P. D. Fainstein, Phys. Rev. A **74**, 060701(R) (2006).
[37] M. R. Chowdhury and L. C. Tribedi, J. Phys. B **50**, 155201 (2017).
[38] R. K. Kushawaha, M. Patanen, R. Guillemin, L. Journel, C. Miron, M. Simon, M. N. Piancastelli, C. Skates, and P. Decleva, Proc. Natl. Acad. Sci. U.S.A. **110**, 15201 (2013).